

Article

The Single-Scattering Albedo of Black Carbon Aerosols in China

Xiaolin Zhang ^{1,2,*}  and Yuanyuan Wu ¹

¹ China Meteorological Administration Aerosol-Cloud and Precipitation Key Laboratory, School of Atmospheric Physics, Nanjing University of Information Science and Technology, Nanjing 210044, China; 202083300921@nuist.edu.cn

² Key Laboratory of Meteorological Disaster, Ministry of Education (KLME), Nanjing University of Information Science and Technology, Nanjing 210044, China

* Correspondence: xlnzhang@nuist.edu.cn

Abstract: Black carbon (BC) aerosols have attracted wide attention over the world due to their significant climate effects on local and global scales. BC extinction aerosol optical thickness (AOT), scattering AOT, and single scattering albedo (SSA) over China are systematically studied based on the MERRA-2 satellite reanalysis data from 1983 to 2022 in terms of the spatial, yearly, seasonal, and monthly variations. The extinction and scattering AOTs of BC show similar spatial distribution, with high values in eastern and southern China, generally as opposed to BC SSA. A decrease in BC extinction and scattering AOTs has been documented over the last decade. The mean BC extinction AOT, scattering AOT, and SSA over China are 0.0054, 0.0014, and 0.26, respectively. The BC SSA showed small variations during 1983–2022, although a high BC extinction AOT and scattering AOT have been seen in the last two decades. During different decades, the seasonal patterns of BC extinction and scattering AOTs may differ, whereas the BC SSA shows seasonal consistency. Significant monthly variations in the BC SSA are seen over four decades, which are in agreement with their seasonal patterns. The mean BC extinction AOTs are 0.037, 0.033, 0.023, and 0.0054, whereas the average BC scattering AOTs are 0.0088, 0.0082, 0.0060, and 0.0014 in the Pearl River Delta (PRD), Yangtze River Delta (YRD), Beijing–Tianjin–Hebei (BTH) region, and Tarim Basin (TB), respectively. It is interesting to see that BC SSA values in the TB region are generally higher than those over the PRD, YRD and BTH areas, whereas the reverse is true for BC extinction and scattering AOTs. This study provides references for further research on black carbon aerosols and air pollution in China.



Citation: Zhang, X.; Wu, Y. The Single-Scattering Albedo of Black Carbon Aerosols in China. *Atmosphere* **2024**, *15*, 1238. <https://doi.org/10.3390/atmos15101238>

Academic Editor: Muhammad Ibrahim

Received: 17 September 2024

Revised: 11 October 2024

Accepted: 14 October 2024

Published: 16 October 2024



Copyright: © 2024 by the authors. Licensee MDPI, Basel, Switzerland. This article is an open access article distributed under the terms and conditions of the Creative Commons Attribution (CC BY) license (<https://creativecommons.org/licenses/by/4.0/>).

Keywords: black carbon; single-scattering albedo; spatial and temporal variations; China

1. Introduction

Black carbon (BC) is one of the components of atmospheric aerosols, mainly produced by the incomplete combustion of carbon-containing substances [1]. Brown carbon is another carbonaceous aerosol, being one of the components of BC organic coatings and absorbing radiations in the ultraviolet and visible spectra [1]. A large number of studies have shown that black carbon aerosols can directly or indirectly impact the atmospheric radiation forcing process and can also be used as a cloud condensation core to indirectly affect the radiation balance between the earth and the atmosphere through the cloud microphysics process, and they have an important impact on global warming [2]. In addition, black carbon aerosols, along with other pollutants, can enter the human body, seriously endangering human health [3]. Therefore, the in-depth study of black carbon aerosols has important scientific significance and social value.

The World Meteorological Organization's Global Atmospheric Monitoring Network has observed black carbon aerosols as an important observation project since 1989. Wu et al. [4] simulate the radiation effect of black carbon aerosols in China and conclude that the largest degree of radiative forcing in the south appears in spring and that in the north appears in summer. Regarding the global distribution of the optical thickness of black carbon aerosols,

Ma et al. [5] conclude that the scattering coefficient and absorption coefficient of black carbon aerosols are of the same order of magnitude in the short wavelength range of less than 0.5 μm . Zhuang et al. [6] analyze aerosol climate effects in China and find that the optical thickness of absorptive aerosols is mainly distributed in northwestern, southwestern, and eastern China. Wei et al. [7] show the distribution and change characteristics of black carbon concentrations in Hefei, exhibiting that the concentrations of black carbon in Hefei are low in spring and summer and high in autumn and winter. Although previous research on black carbon source emissions and climate effects has been carried out intensively, the study of black carbon's optical properties, such as the single-scattering albedo over China, is still limited, which would hopefully be beneficial to improving the air quality in China and providing references for climate changes and climate assessments, and people's happiness index is of great significance.

Here, the spatial and temporal characteristics of the BC single-scattering albedo over China during the period of 1983–2022 based on MERRA-2 satellite reanalysis data are systematically measured. The characteristics of BC extinction and the scattering optical thicknesses are also explored. This paper is organized as follows. In Section 2, the MERRA-2 data for BC's optical properties are introduced. In Section 3, the 40-year detailed characteristics of BC extinction, scattering optical thicknesses, and single-scattering albedo are discussed. Finally, in Section 4, the main conclusions are summarized.

2. Methodology

2.1. MERRA-2 Dataset

The MERRA-2 data are a series of long-term reanalysis datasets developed by the NASA Goddard Space Flight Center. MERRA-2 uses the Goddard Earth Observing System Model (GEOS), and aerosols in MERRA-2 are simulated with a radiatively coupled version of the Goddard Chemistry, Aerosol, Radiation, and Transport model (GOCART) [8]. Data for an aerosol total optical thickness of 550 nm is obtained from the Moderate Resolution Imaging Spectroradiometer (MODIS), and the MERRA-2 collection consists of assimilated aerosol diagnostics, such as black carbon extinction and scattering optical thicknesses. The MERRA-2 data provide lattice data with a spatial resolution of $0.5^\circ \times 0.625^\circ$ and a time span from 1 January 1980 to the present [8]. We employed a black carbon extinction aerosol optical thickness (AOT) and scattering AOT of 550 nm on the basis of the MERRA-2 reanalysis products. The single-scattering albedo (SSA) of black carbon aerosols was then calculated and defined as the ratio of the scattering AOT to the extinction AOT of BC. In addition to brown carbon, BC and dust are two significant absorbing aerosols, but BC and dust have different source regions, optical properties, and sizes [9]. Mineral dust mostly originates from arid regions, such as the Gobi and Taklimakan deserts, whereas BC is generally emitted from fossil fuel combustion and biomass burning [10]. Moreover, BC is generally smaller than dust, while BC particles are more absorbing than dust particles. The stronger absorption characteristics of BC result in a lower BC SSA compared to that of dust [11].

2.2. Targeted Area

We focus on the characteristics of BC's extinction AOT, scattering AOT, and SSA in China, especially in the Tarim Basin (TB), Pearl River Delta (PRD), Yangtze River Delta (YRD), and Beijing–Tianjin–Hebei (BTH) region, which are portrayed in Figure 1. With the rapid economic developments of the PRD, YRD, and BTH regions, plenty of black carbon aerosols are emitted in these areas. However, the Tarim Basin, inside Taklimakan Desert, has low BC emissions.

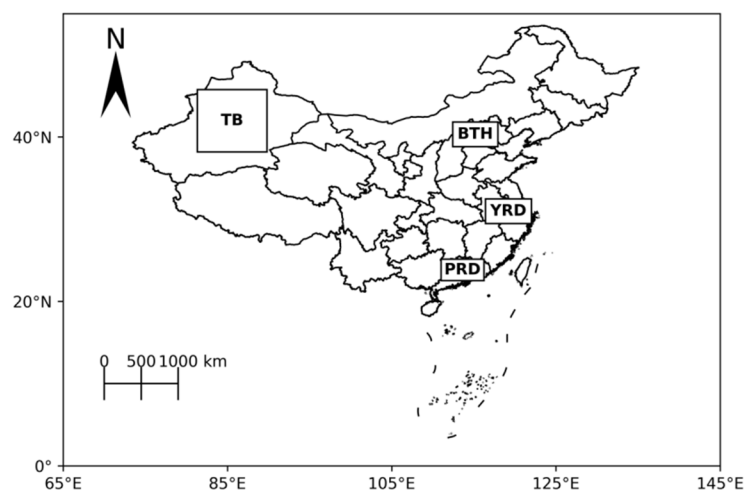


Figure 1. Locations of study areas in China. The Tarim Basin (TB, region: $36\text{--}45^\circ\text{ N}$, $80\text{--}91^\circ\text{ E}$), Pearl River Delta (PRD, region: $22\text{--}24^\circ\text{ N}$, $112\text{--}115^\circ\text{ E}$), Yangtze River Delta (YRD, region: $29\text{--}33^\circ\text{ N}$, $117\text{--}122^\circ\text{ E}$), and Beijing–Tianjin–Hebei region (BTH, region: $38\text{--}41^\circ\text{ N}$, $114\text{--}119^\circ\text{ E}$) are considered four representative regions in China in the study.

3. Results and Discussion

3.1. Spatial Distributions of BC's Extinction and Scattering AOTs and SSA

The spatial distributions of BC's extinction AOT, scattering AOT, and SSA in China from 1983 to 2022 are portrayed in Figure 2. Four decades, 1983–1992, 1993–2002, 2003–2012, and 2013–2022, are shown from left to right, while the extinction AOT, scattering AOT, and SSA of BC are shown from top to bottom. As illustrated in Figure 2a–d, BC's extinction AOTs in eastern China and southern China are significantly higher than those in western China and northern China. BC extinction AOT values as high as 0.05 are seen in eastern China and southern China, while they are less than 0.015 in western China and northern China. This is probably associated with fast economic development generating plenty of black carbon emissions over eastern and southern China over the last four decades [12]. A high BC extinction AOT of nearly 0.05 is seen over the Sichuan Basin, and this may be due to terrain reasons [13]. Significant decadal variations in BC's extinction AOT are observed, and high BC extinction AOTs are seen during 2003–2012, especially in the Beijing–Tianjin–Hebei region, Yangtze River Delta, and Sichuan Basin. Meanwhile, a decrease in BC's extinction AOT is seen in the final decade (i.e., during 2013–2022). Zhou et al. [14] also show high BC levels in the Sichuan Basin associated with continuously increasing extinction optical thickness.

As shown in Figure 2e–h, BC's scattering AOTs show similar spatial distribution and decadal variation patterns to those of BC's extinction AOTs. BC scattering AOTs as high as 0.018 are seen during 2003–2012, indicating that industrial development leads to the emissions of scattering particles, such as sulfate and nitrate particles [15]. The low BC extinction AOTs in western China and northern China are attributed to small emissions of BC aerosols. A decrease in BC's scattering AOT is also seen during 2013–2022, and this may be because of the implementation of environmental protection policies in the last decade [16,17].

As shown in Figure 2i–l, the SSA of black carbon aerosols in China is between 0.20 and 0.31. High BC SSA values, exceeding 0.28, are observed in northern Heilongjiang Province, the northeast Inner Mongolia Autonomous Region, southern Qinghai Province, the southern Xinjiang Uygur Autonomous Region, the northern Tibet Autonomous Region, and northwest Sichuan Province. However, low BC SSA values, less than 0.24, are seen in the Henan, Shandong, and Hebei provinces, and this may indicate high absorption levels in these areas. BC's SSA generally exhibits an opposite spatial distribution to BC's extinction and scattering AOTs. Large BC emissions in eastern China and southern China result in high BC extinction and scattering AOTs, while plenty of other carbonaceous

aerosols (such as brown carbon) may also be emitted. These brown carbon aerosols show absorption at some wavelengths and may contribute to the high BC SSA in eastern China and southern China.

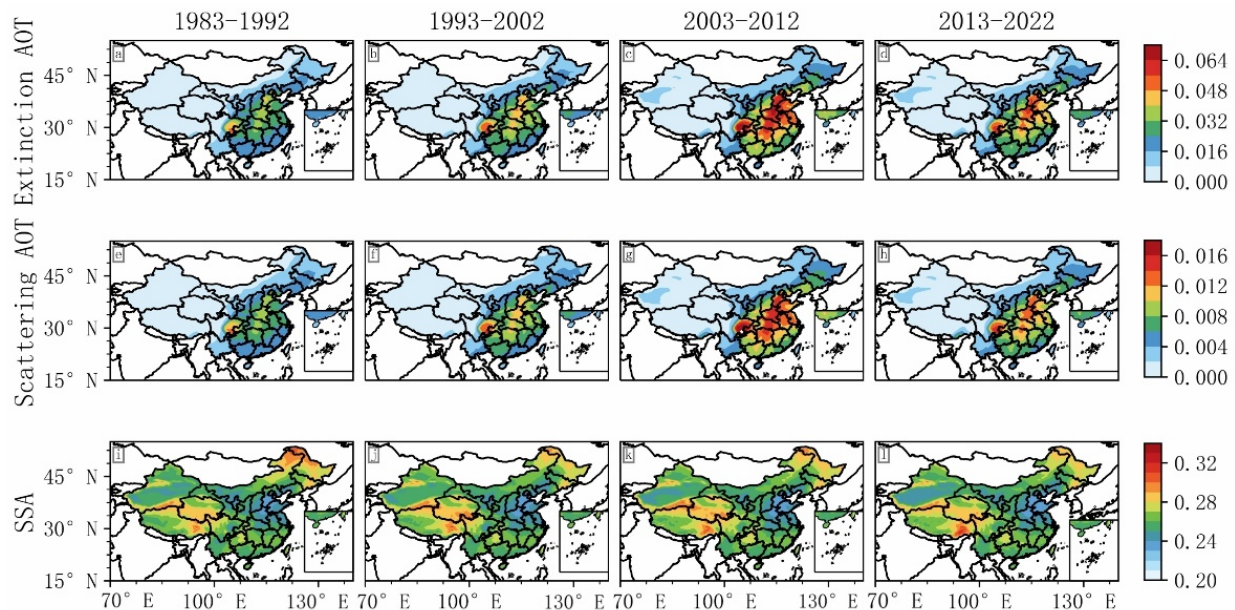


Figure 2. Spatial distributions of the extinction AOT (a–d), scattering AOT (e–h), and SSA (i–l) of black carbon aerosols over China. Four decades, 1983–1992 (a,e,i), 1993–2002 (b,f,j), 2003–2012 (c,g,k) and 2013–2022 (d,h,l), are shown.

To summarize, BC's extinction and scattering AOTs show similar spatial distribution patterns with high values in eastern and southern China, generally opposing that of BC's SSA. A decrease in BC's extinction and scattering AOTs has been documented over the last decade, and this may indicate the implementation of environmental protection policies.

3.2. Annual Variations in BC's Extinction and Scattering AOTs and SSA

The time series of the yearly mean black carbon extinction AOT, scattering AOT, and SSA over China during 1983–2022 are illustrated in Figure 3. BC's extinction AOT generally exhibits well-defined yearly variations. The yearly average BC extinction AOT values changed from 0.0038 to 0.0079 during 1983–2022, with a mean value of 0.0054. The lowest BC extinction AOT values are probably associated with precipitation events, as precipitation is one of the removal mechanisms for black carbon aerosols [18]. The highest BC extinction AOT could be associated with BC episodes induced by anthropogenic traffic and industrial emissions, biomass burning, and synoptic weather patterns [19].

The annual values of BC's scattering AOT range from 0.0008 to 0.0017, with a mean of 0.0014, and are shown in Figure 3b. Before 1998, the annual average level of BC's scattering AOT was relatively low, with values fluctuating around 0.0009. During 1999–2022, high scattering AOTs were seen, with values between 0.0009 and 0.0017.

As shown in Figure 3c, the annual average SSA of black carbon aerosols is between 0.26 and 0.27, with a mean value of 0.264. This may be related to the relatively small effect of BC emissions on BC's SSA, especially for medium to high altitudes below the satellite altitude [20]. Overall, the mean BC extinction AOT, scattering AOT, and SSA over China during 1983–2022 were 0.0054, 0.0014, and 0.264, respectively. BC's SSA showed small variations during 1983–2022, although a high BC extinction AOT and scattering AOT have been seen over the last two decades, probably indicating that the ratio of BC to sulfur emissions has remained approximately constant.

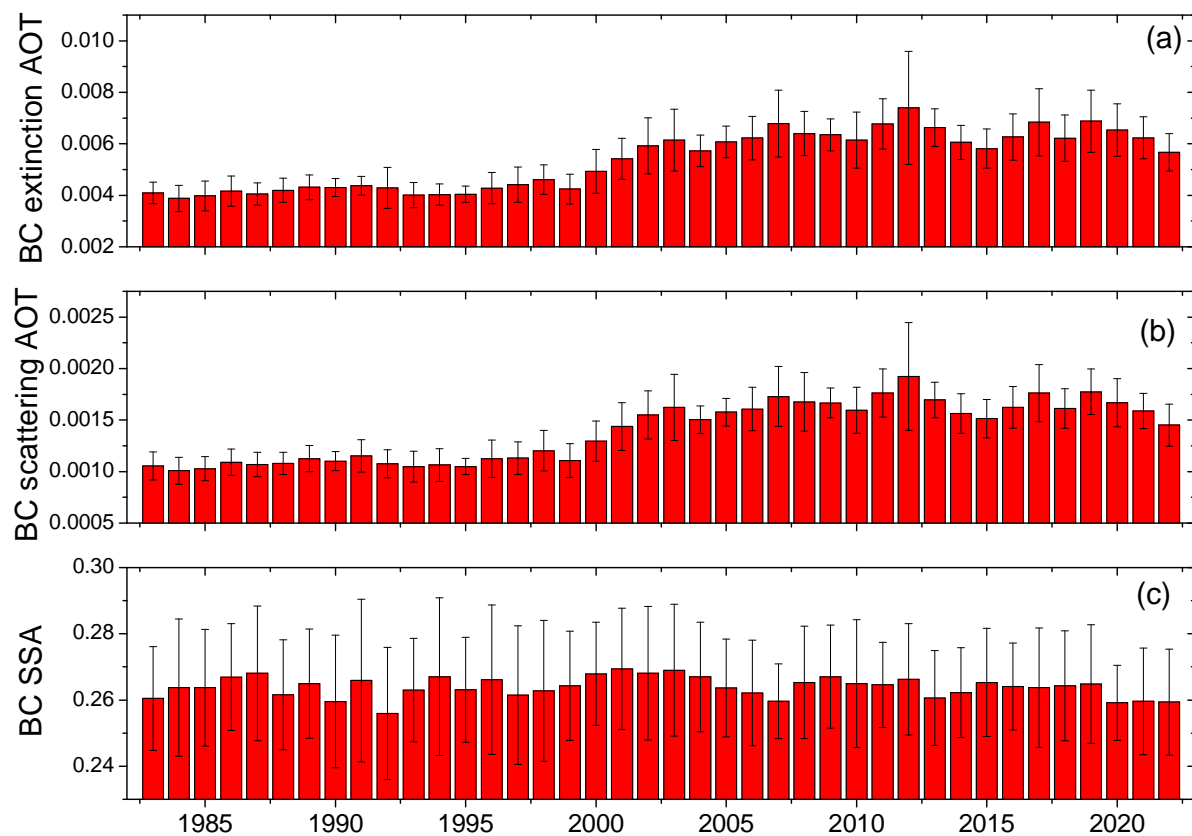


Figure 3. Temporal variations in annual average BC extinction AOT (a), scattering AOT (b), and SSA (c) over China from 1983 to 2022. Uncertainty bars are the standard deviations related to the mean values.

3.3. Seasonal Patterns of BC Extinction and Scattering AOTs and SSA

The seasonal variations in BC's extinction AOT, scattering AOT, and SSA over China from 1983 to 2022 are shown in Figure 4. As shown in Figure 4a, similar seasonal patterns for the extinction AOT are observed in different decades. The largest extinction AOT is observed in summer, followed by autumn and winter, and the spring has the smallest extinction AOT. The high extinction AOT in summer may be attributed to biomass burning due to crop harvesting [21]. For the scattering AOT, different seasonal patterns are shown in the different decades during the last three decades. During 1983–2002, the scattering AOT was lowest in autumn and highest in spring. During 2003–2012, the scattering AOT was largest in summer and smallest in autumn. However, during 2013–2022, the smallest scattering AOT was seen in spring, while the highest value was observed in winter (see Figure 4b). The high scattering AOT in winter may be attributed to the coal widely used in northern China, in addition to the frequent temperature inversion and strong atmospheric stability [22,23].

The BC's SSA has a similar seasonal variability over the four decades, which is illustrated in Figure 4c. The spring had the largest BC SSA, followed by winter and fall, while the summer had a relatively lower BC SSA. The seasonally averaged BC SSA in the period of 2013–2022 was 0.28, 0.25, 0.26, and 0.27 for spring, summer, fall, and winter, respectively. Moreover, the seasonal pattern of BC's SSA in China basically does not change over a decade. In general, during different decades, the seasonal patterns of BC's extinction and scattering AOTs may differ, whereas BC's SSA shows seasonal consistency.

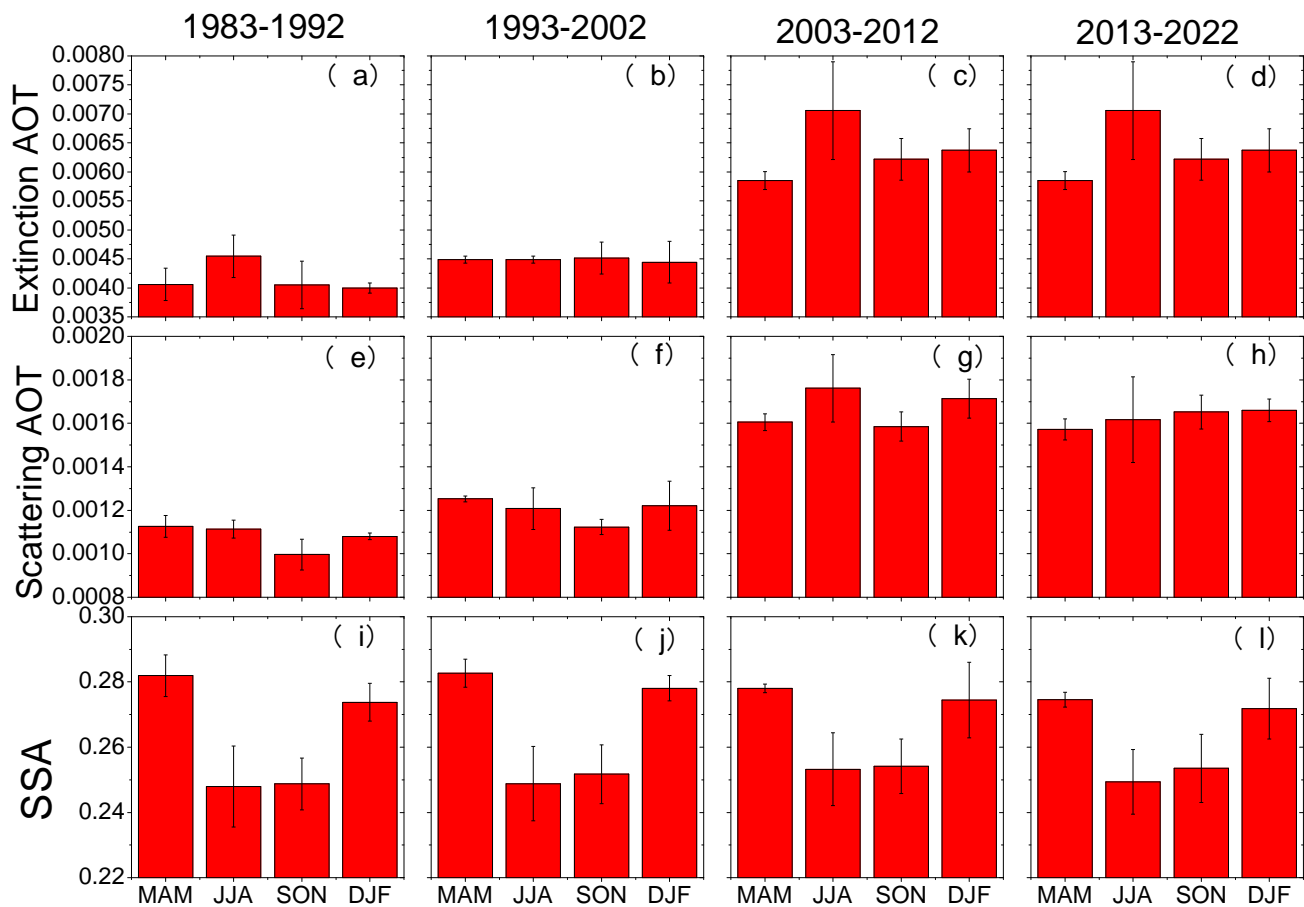


Figure 4. Seasonal average BC extinction AOT, scattering AOT, and SSA over mainland China in spring (MAM), summer (JJA), fall (SON), and winter (DJF). The results for the periods 1983–1992 (a,e,i), 1993–2002 (b,f,j), 2003–2012 (c,g,k), and 2013–2022 (d,h,l) are shown.

3.4. Monthly Variations in BC's Extinction and Scattering AOTs and SSA

The monthly mean variations in BC's extinction AOT, scattering AOT, and SSA from 1983 to 2022 are provided in Figure 5. The monthly mean BC extinction and scattering AOTs in the period of 2003–2012 are significantly higher than those during 1983–2002. The monthly average extinction AOT of BC varies almost twofold, ranging from 0.0057 in March to 0.0078 in July. The monthly pattern of BC's scattering AOT shows complexity in different decades, with the highest BC scattering AOT being 0.0017 reached in November and the lowest being 0.0014 in June during 2013–2022.

As illustrated in Figure 5i–l, significant monthly variations in BC's SSA are seen during the four decades, which are consistent with their seasonal patterns. From 1983 to 2022, the highest monthly mean BC SSA was seen in February or March, while the lowest BC SSA was seen in July or August. The minimum BC SSA was 0.24 in July and the maximum was 0.28 in February during 2013–2022.

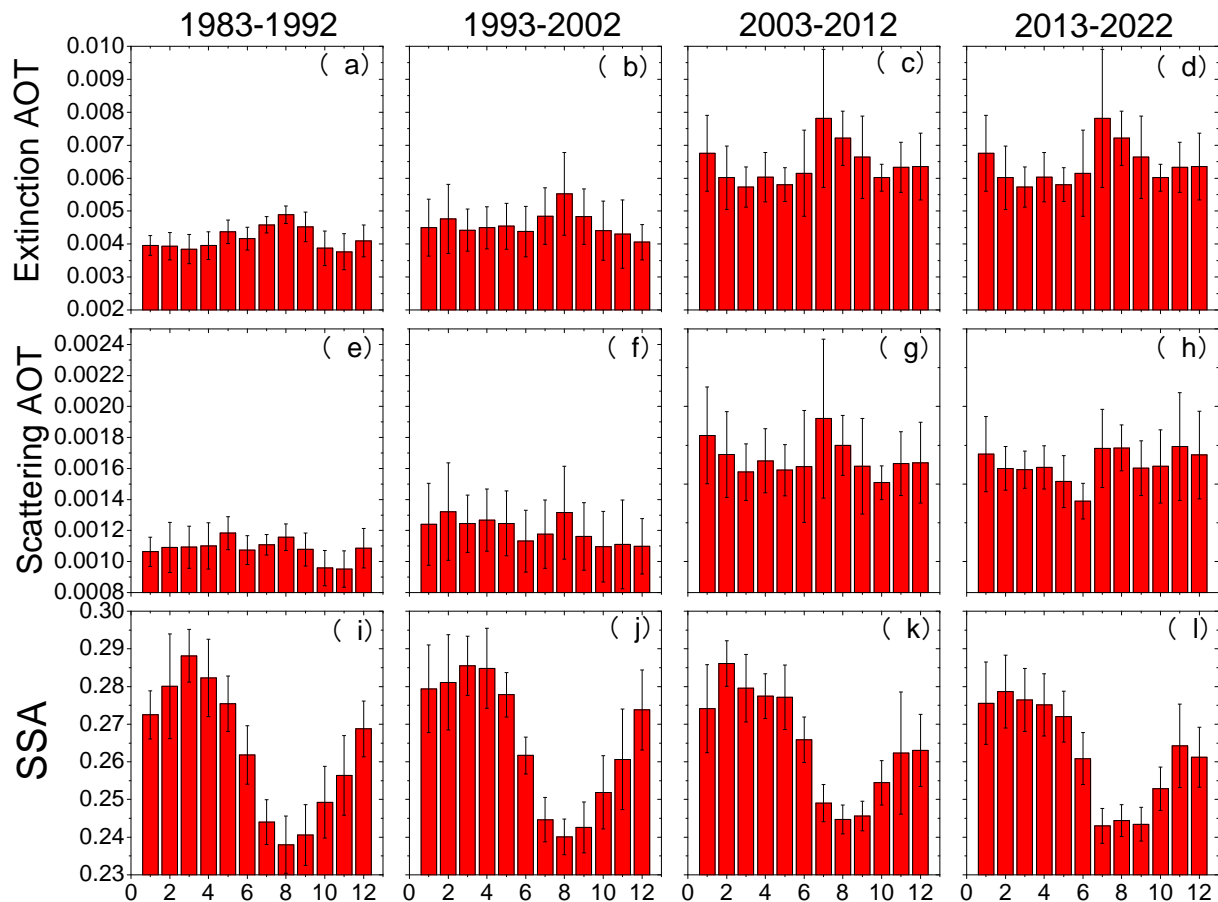


Figure 5. Monthly average BC extinction AOT (a–d), scattering AOT (e–h), and SSA (i–l) over mainland China. The results for the periods 1983–1992 (a,e,i), 1993–2002 (b,f,j), 2003–2012 (c,g,k), and 2013–2022 (d,h,l) are shown.

3.5. BC's Extinction and Scattering AOTs and SSA in Typical Regions of China

To further understand the characteristics of BC's SSA and AOT in China, four typical areas, including the TB region, with few BC particles, and the PRD, YRD, and BTH regions, dominated by anthropogenic BC aerosols, are considered. The annual variations in BC's extinction AOT, scattering AOT, and SSA are shown in Figure 6. The mean BC extinction AOTs in the BTH, YRD, PRD, and TB regions are 0.037, 0.033, 0.023, and 0.0054, respectively. Meanwhile, the average BC scattering AOTs are 0.0088, 0.0082, 0.0060, and 0.0014 over the BTH, YRD, PRD, and TB regions, respectively. BC's SSA in the BTH, YRD, PRD, and TB regions are 0.24, 0.25, 0.26, and 0.26, respectively. It is shown that the annual mean extinction AOT and scattering AOT of BC in the PRD, YRD, and BTH regions have similar variation patterns, with high values during 2003–2012 and low levels during 1983–1992, which are significantly larger than those over the TB region. In the BTH, YRD, PRD, and TB regions, the maximum values of BC's extinction AOT are 0.055, 0.048, 0.036, and 0.01, respectively, while the maximum BC scattering AOTs are 0.013, 0.014, 0.009, and 0.002, respectively. The high values of BC's AOTs over the BTH, YRD, and PRD regions are probably due to the substantial increases in BC emissions in the period of 2003–2012. BC's SSAs in the BTH, YRD, PRD, and TB regions are in the ranges of 0.24–0.25, 0.26–0.27, 0.25–0.26, and 0.26–0.27, respectively. It is interesting to see that BC's SSA values in the TB region are generally higher than those over the PRD, YRD, and BTH areas, whereas the reverse is true for BC's extinction and scattering AOTs.

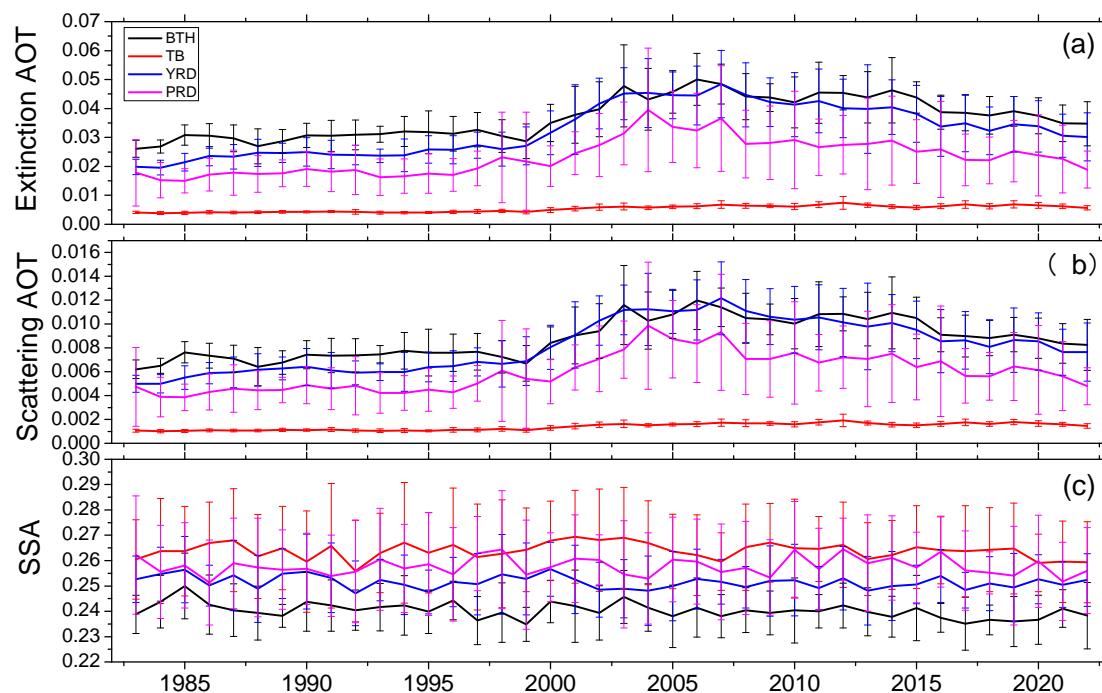


Figure 6. Temporal variations in annual average BC extinction AOT (a), scattering AOT (b), and SSA (c) over the TB, PRD, YRD, and BTH regions from 1983 to 2022.

The seasonally averaged extinction AOT, scattering AOT, and SSA of BC over the representative four areas of China are illustrated in Figure 7. BC's extinction AOT and scattering AOT in the BTH region present high values in summer and autumn and low values in spring and winter. High temperatures, abundant water vapor content, and more straightforward photochemical reactions are seen in summer [24,25]. A large amount of straw burning may be one of the reasons for the high BC AOT in summer. The values of BC's extinction and scattering AOTs in the YRD and PRD regions are low in summer and autumn and high in spring and winter. Generally, similar seasonal patterns of BC's extinction and scattering AOTs in the PRD, YRD, and BTH regions are seen in the different decades. The seasonal variations in BC's extinction and scattering AOTs in the Tarim Basin are not obvious due to their relatively low values. The BC SSA seasonal patterns in the four regions generally differ from each other and are also different from the patterns obtained for China overall. This indicates the complicated characteristics of the BC emissions and meteorological conditions over the different regions. High concentrations of biomass burning from natural surfaces are seen in the Tarim Basin [26]. Desert dust is weakly absorbing, and the SSAs of transported dust from the Taklimakan Desert at 530 nm are between 0.80 and 0.90 based on ground measurements in Beijing and Tsukuba [27]. The SSA of the Sahara desert dust increases with wavelength, from 0.81 ± 0.05 at 415.6 nm to 0.94 ± 0.05 at 868.7 nm [28]. The mixing of BC with dust may induce uncertainties in BC's SSA values.

The decadal variations in the monthly averaged extinction AOT, scattering AOT, and SSA of BC in four regions in the period of 1983–2022 are shown in Figure 8. Large monthly mean values of BC's AOT are generally seen during 2003–2012, while the monthly patterns of BC's extinction AOT, scattering AOT, and SSA in the four areas are similar in the different decades. Furthermore, the monthly patterns for the extinction AOT, scattering AOT, and SSA of BC over different areas have discrepancies. This suggests the complexity of the monthly characteristics of BC optics, consistent with their seasonal patterns in various regions.

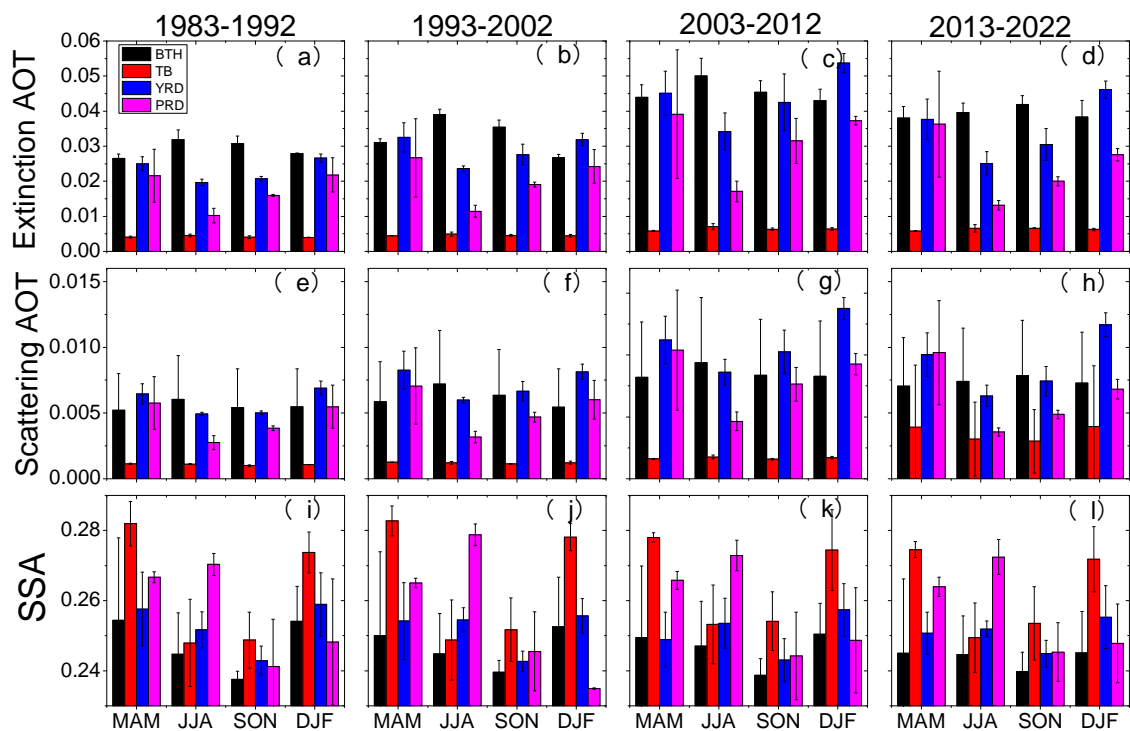


Figure 7. Seasonal average BC extinction AOT (a–d), scattering AOT (e–h), and SSA (i–l) in the TB, PRD, YRD, and BTH regions in spring (MAM), summer (JJA), fall (SON), and winter (DJF). Results during 1983–1992 (a,e,i), 1993–2002 (b,f,j), 2003–2012 (c,g,k), and 2013–2022 (d,h,l) are shown.

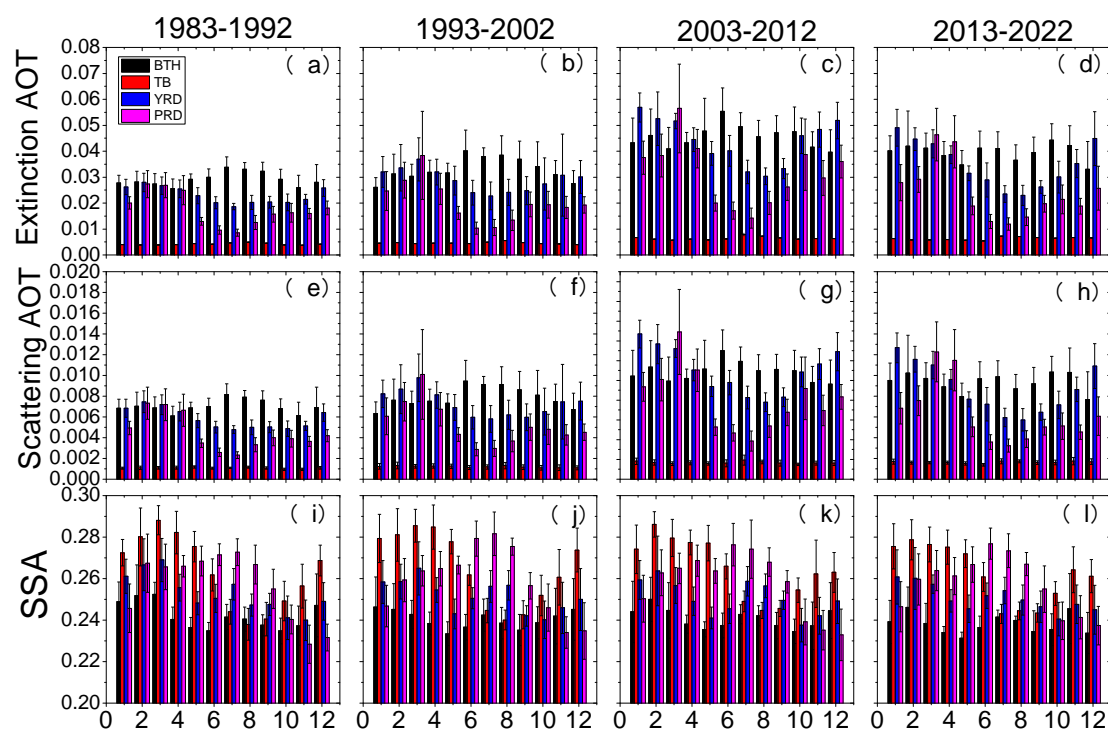


Figure 8. Monthly average BC extinction AOT (a–d), scattering AOT (e–h), and SSA (i–l) in the TB, PRD, YRD, and BTH regions. Results in the periods of 1983–1992 (a,e,i), 1993–2002 (b,f,j), 2003–2012 (c,g,k), and 2013–2022 (d,h,l) are considered.

4. Conclusions

In this paper, MERRA-2 satellite reanalysis data are employed to study BC's extinction and scattering AOTs and SSA in China from 1983 to 2022 in terms of their spatial, yearly, seasonal, and monthly variations. BC's extinction and scattering AOTs and SSA in typical regions of China are also explored.

The extinction and scattering AOTs of BC show similar spatial distribution patterns with high values in eastern and southern China, generally as opposed to BC's SSA. A decrease in BC's extinction and scattering AOTs has been documented over the last decade, and this indicates the implementation of environmental protection policies. The mean BC extinction AOT, scattering AOT, and SSA over China during 1983–2022 were 0.0054, 0.0014, and 0.264, respectively. BC's SSA also showed small variations during 1983–2022, although a high BC extinction AOT and scattering AOT have been seen over the last two decades. This probably indicates the variations in aerosol composition and emission patterns and the existence of dust aerosols [8]. During the different decades, the seasonal patterns of BC's extinction and scattering AOTs may differ, whereas BC's SSA shows seasonal consistency. Significant monthly variations in BC's SSA were seen during the four decades, which are in agreement with seasonal patterns.

The mean BC extinction AOTs in the BTH, YRD, PRD, and TB regions are 0.037, 0.033, 0.023, and 0.0054, respectively. Meanwhile, the average BC scattering AOTs are 0.0088, 0.0082, 0.0060, and 0.0014 over the BTH, YRD, PRD, and TB regions, respectively. BC's SSA in the BTH, YRD, PRD, and TB regions is 0.24, 0.25, 0.26, and 0.26, respectively. It is interesting to see that BC's SSA values in the TB are generally higher than those over the PRD, YRD, and BTH regions, whereas the reverse is true for BC's extinction and scattering AOTs.

Author Contributions: Conceptualization, X.Z.; methodology, X.Z.; software, Y.W. and X.Z.; validation, X.Z.; formal analysis, Y.W. and X.Z.; investigation, Y.W. and X.Z.; resources, X.Z.; data curation, Y.W. and X.Z.; writing—original draft preparation, Y.W.; writing—review and editing, X.Z.; visualization, Y.W. and X.Z.; supervision, X.Z.; project administration, X.Z.; funding acquisition, X.Z. All authors have read and agreed to the published version of the manuscript.

Funding: This work is part of the Qinglan Project and is also supported by the State Key Laboratory of Atmospheric Boundary Layer Physics and Atmospheric Chemistry (LAPC-KF-2023-09) and China Meteorological Administration Atmospheric Chemistry Key Laboratory (2024B05).

Institutional Review Board Statement: Not applicable.

Informed Consent Statement: Not applicable.

Data Availability Statement: The data presented in this study are available on request from the corresponding author. The data are not publicly available due to privacy.

Acknowledgments: The analyses and visualizations used in this paper were produced with the Giovanni online data system and developed and maintained by the NASA GES DISC. We also acknowledge the mission scientists and Principal Investigators who provided the data used in this research effort.

Conflicts of Interest: The authors declare no conflict of interest.

References

1. Zhang, X.; Rao, R.; Huang, Y.; Mao, M.; Berg, M.; Sun, W. Black carbon aerosols in urban central China. *J. Quant. Spectrosc. Radiat. Transf.* **2015**, *150*, 3–11. [\[CrossRef\]](#)
2. Biagio, C.D.; Sarra, A.D.; Meloni, D. Large atmospheric shortwave radiative forcing by Mediterranean aerosols derived from simultaneous ground-based and spaceborne observations and dependence on the aerosol type and single scattering albedo. *J. Geophys. Res. Atmos.* **2010**, *115*, D10209. [\[CrossRef\]](#)
3. Huang, X.; Ding, A.; Wang, Z.; Ding, K.; Gao, J.; Chai, F.; Fu, C. Amplified transboundary transport of haze by aerosol–boundary layer interaction in China. *Nature* **2020**, *13*, 428–434. [\[CrossRef\]](#)
4. Wu, J.; Fu, C. Simulation study of distribution transmission and radiation effect of black carbon aerosol in East Asian spring in the past five years. *Atmos. Sci.* **2005**, *29*, 111–119.

5. Zhang, X.; Huang, Y.; Zhu, W.; Rao, R. Aerosol characteristics during summer haze episodes from different source regions over the coast city of North China Plain. *J. Quant. Spectrosc. Radiat. Transf.* **2013**, *122*, 180–193. [\[CrossRef\]](#)
6. Mao, M.; Zhou, Y.; Zhang, X. Evaluation of MERRA-2 Black Carbon Characteristics and Potential Sources over China. *Atmosphere* **2023**, *14*, 1378. [\[CrossRef\]](#)
7. Zhang, X.; Wang, Y.; Zhou, Y.; Wang, J.; Mao, M. Significance of Absorbing Fraction of Coating on Absorption Enhancement of Partially Coated Black Carbon Aerosols. *Atmosphere* **2021**, *12*, 1422. [\[CrossRef\]](#)
8. Randles, C.A.; Silva, A.M.D.; Buchard, V.; Colarco, P.R.; Darmenov, A.; Govindaraju, R.; Smirnov, A.; Holben, B.; Ferrare, R.; Hair, J.; et al. The MERRA-2 Aerosol Reanalysis, 1980 Onward. Part I: System Description and Data Assimilation Evaluation. *J. Clim.* **2017**, *30*, 6823–6850. [\[CrossRef\]](#)
9. Zhang, X.; Mao, M.; Yin, Y.; Tang, S. The absorption Angstrom exponent of black carbon with brown coatings: Effects of aerosol microphysics and parameterization. *Atmos. Chem. Phys.* **2020**, *20*, 9701–9711. [\[CrossRef\]](#)
10. DeLessio, M.A.; Tsigaridis, K.; Bauer, S.E.; Chowdhary, J.; Schuster, G.L. Modeling atmospheric brown carbon in the GISS ModelE Earth system model. *Atmos. Chem. Phys.* **2024**, *24*, 6275–6304. [\[CrossRef\]](#)
11. Zhang, X.; Mao, M.; Chen, H.; Tang, S. The single scattering albedo Angstrom exponent of black carbon with brown coatings. *J. Quant. Spectrosc. Radiat. Transf.* **2021**, *259*, 107429. [\[CrossRef\]](#)
12. Zhang, N.; Qin, Y.; Xie, S.D. Spatial distribution of black carbon emissions in China. *Chin. Sci. Bull.* **2013**, *58*, 1855–1864. [\[CrossRef\]](#)
13. Yuan, L.; Zhang, X.L.; Che, Y.Z.; Xia, X.; Liu, X.; Zhao, T.; Song, M. Vertical profile and radiative forcing of black carbon in a winter pollution period over Chengdu, China. *Atmos. Res.* **2022**, *265*, 105896. [\[CrossRef\]](#)
14. Mao, M.; Jiang, H.; Zhang, X. Spatiotemporal Variation in Absorption Aerosol Optical Depth over China. *Atmosphere* **2024**, *15*, 1099. [\[CrossRef\]](#)
15. Cai, Z.; Cai, Y.; Ying, Z.; Qin, H.; He, H.; Qing, Y. Observation and study of black carbon aerosols and their absorption characteristics in Tianjin. *China Environ. Sci.* **2011**, *31*, 719–723.
16. Yuan, X.; Zuo, J. Transition to low carbon energy policies in China—From the Five-Year Plan perspective. *Energy Policy* **2011**, *39*, 3855–3859. [\[CrossRef\]](#)
17. Zhang, X.; Zhou, Y. Aerosol direct radiative forcing over China: A 40-year MERRA-2-based evaluation. *Atmos. Environ.* **2023**, *299*, 119659. [\[CrossRef\]](#)
18. Zhang, X.L.; Huang, Y.B.; Rao, R.Z. Aerosol characteristics including fumigation effect under weak precipitation over the southeastern coast of China. *J. Atmos. Sol. Terr. Phys.* **2012**, *84–85*, 25–36. [\[CrossRef\]](#)
19. Zhang, X.L.; Huang, Y.B.; Rao, R.Z.; Wang, Z.E. Retrieval of effective complex refractive index from intensive measurements of characteristics of ambient aerosols in the boundary layer. *Opt. Express* **2013**, *21*, 17849–17862. [\[CrossRef\]](#)
20. Zhang, X.; Xu, M. Aerosol column single scattering albedos over the Yangtze Delta region. *J. Nanjing Univ. Form. Sci. Technol. (Nat. Sci. Ed.)* **2021**, *13*, 252–256.
21. Cao, J.J.; Wu, F.; Chow, J.C.; Lee, S.C.; Li, Y.; Chen, S.W.; An, Z.S.; Fung, K.K.; Watson, J.G.; Zhu, C.S.; et al. Characterization and source apportionment of atmospheric organic and elemental carbon during fall and winter of 2003 in Xi'an, China. *Atmos. Chem. Phys.* **2005**, *5*, 3561–3593. [\[CrossRef\]](#)
22. Mao, R.; Gong, D.; Shao, Y.; Wu, G.; Bao, J. Numerical analysis for contribution of the Tibetan Plateau to dust aerosols in the atmosphere over the East Asia. *Sci. China Earth Sci.* **2013**, *56*, 301–310. [\[CrossRef\]](#)
23. Zhou, Y.; Zhang, X.; Wang, Y. High Wet Deposition of Black Carbon over the Sichuan Basin of China. *Atmosphere* **2023**, *14*, 598. [\[CrossRef\]](#)
24. Lei, Y.; Zhang, Q.; He, K.B.; Streets, D.G. Primary anthropogenic aerosol emission trends for China, 1990–2005. *Atmos. Chem. Phys.* **2011**, *11*, 931–954. [\[CrossRef\]](#)
25. Zhang, X.; Mohammed, A.H.A.; Zhou, Y.; Mao, M. Dry Deposition of Hydrophilic Black Carbon Aerosols in China. *Atmosphere* **2023**, *14*, 1114. [\[CrossRef\]](#)
26. Zhang, X.; Mao, M.; Chen, H.; Yin, Y.; Tang, S. Lensing Effect of Black Carbon With Brown Coatings: Dominant Microphysics and Parameterization. *J. Geophys. Res. Atmos.* **2021**, *126*, e2020JD033549. [\[CrossRef\]](#)
27. Uchiyama, A.; Yamazaki, A.; Togawa, H.; Asano, J.; Shi, G. Single Scattering Albedo of Aeolian Dust as Inferred from Sky-radiometer and in situ Ground-based Measurement. *Sci. Online Lett. Atmos. (SOLA)* **2005**, *1*, 209–212. [\[CrossRef\]](#)
28. Meloni, D.; di Sarra, A.; Pace, G.; Monteleone, F. Aerosol optical properties at Lampedusa (Central Mediterranean). 2. Determination of single scattering albedo at two wavelengths for different aerosol types. *Atmos. Chem. Phys.* **2006**, *6*, 715–727. [\[CrossRef\]](#)

Disclaimer/Publisher's Note: The statements, opinions and data contained in all publications are solely those of the individual author(s) and contributor(s) and not of MDPI and/or the editor(s). MDPI and/or the editor(s) disclaim responsibility for any injury to people or property resulting from any ideas, methods, instructions or products referred to in the content.